JACS
JOURNAL OF THE AMERICAN CHEMICAL SOCIETY

ARTICLE

pubs.acs.org/JACS

Modular Engineering of H-Bonded Supramolecular Polymers for Reversible Functionalization of Carbon Nanotubes

Anna Llanes-Pallas,[†] K. Yoosaf,[‡] Hassan Traboulsi,[§] John Mohanraj,[‡] Thomas Seldrum,[∥] Jacques Dumont,[∥] Andrea Minoia,[⊥] Roberto Lazzaroni,[*,⊥] Nicola Armaroli,[*,‡] and Davide Bonifazi[*,†,§]

[†]Università di Trieste, Dipartimento di Scienze Chimiche e Farmaceutiche and INSTM UdR di Trieste, Italy

[‡]Molecular Photoscience Group, Istituto per la Sintesi Organica e la Fotoreattività, Consiglio Nazionale delle Ricerche (CNR−ISOF), Bologna, Italy

[§]Department of Chemistry

[∥]Department of Physics

University of Namur (FUNDP), Namur, Belgium,

[⊥]Laboratory for Chemistry of Novel Materials, University of Mons (UMONS), Mons, Belgium

Supporting Information

ABSTRACT: A H-bond-driven, noncovalent, reversible solubilization/functionalization of multiwalled carbon nanotubes (MWCNTs) in apolar organic solvents ($CHCl_3$, CH_2Cl_2, and toluene) has been accomplished through a dynamic combination of self-assembly and self-organization processes leading to the formation of supramolecular polymers, which enfold around the outer wall of the MWCNTs. To this end, a library of phenylacetylene molecular scaffolds with complementary recognition sites at their extremities has been synthesized. They exhibit triple parallel H-bonds between the NH−N−NH (DAD) functions of 2,6-di(acetylamino)pyridine and the CO−NH−CO (ADA) imidic groups of uracil derivatives. These residues are placed at 180° relative to each other (linear systems) or at 60°/120° (angular modules), in order to tune their ability of wrapping around MWCNTs. Molecular Dynamics (MD) simulations showed that the formation of the hybrid assembly **MWCNT•**$[$**X•Y**$]_n$ (where **X** = **1a** or **1b** -DAD- and **Y** = **2**, **3**, or **4** -ADA-) is attributed to $\pi-\pi$ and CH$-\pi$ interactions between the graphitic walls of the carbon materials and the oligophenyleneethynylene polymer backbones along with its alkyl groups, respectively. Addition of polar or protic solvents, such as DMSO or MeOH, causes the disruption of the H-bonds with partial detachment of the polymer from the CNTs, followed by precipitation. Taking advantage of the chromophoric and luminescence properties of the molecular subunits, the solubilization/precipitation processes have been monitored by UV−vis absorption and luminescence spectroscopies. All hybrid MWCNTs−polymer materials have been also structurally characterized via thermogravimetric analysis (TGA), transmission electron microscopy (TEM), atomic force microscopy (AFM), scanning tunneling microscopy (STM), and X-ray photoelectron spectroscopy (XPS).

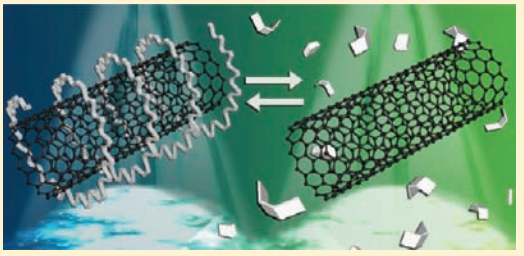

INTRODUCTION

Since their production[1] and subsequent development of mass-production techniques, carbon nanotubes (CNTs) have raised a great deal of interest in a number of different applications such as field-emission devices,[2] molecular electronics,[3] microelectronics,[4] optoelectronics,[5,6] gas storage,[7] sensing,[8] solar cells,[6,9] and, more generally, in nanotechnology. Among the numerous potential applications of CNTs, their uses in the field of nanobiomedicine have recently started to emerge, raising great expectations.[10] For instance, the use of CNTs is becoming relevant in bioimaging, neuroscience, and tissue engineering.[11] To render CNTs processable and allow their widespread use in real applications, chemical functionalization with tailored appended functional groups has been undertaken, enabling the integration of CNTs into multicomponent organic materials.[12] The chemical approaches[13] for the modification of CNTs can be covalent or noncovalent (i.e., supramolecular): while the latter approach does not lead to structural modification of the carbon framework, preserving its key electronic and structural properties, covalent derivatization often leads to substantial structural and physical alterations as a consequence of the rupture of π-conjugation.

In principle, flexible oligomeric and polymeric architectures such as polyaromatic conjugates,[14] polymers,[15] or DNA[16] can provide structures capable of noncovalent wrapping of the CNT surface by exploiting van der Waals and $\pi-\pi$ interactions.[17,18] Notably, some conjugated oligomeric structures may lead to an improvement of the electronic properties, such as conductivities and charge mobility.[19,20] Hence, this approach is extremely versatile for the development of reproducible and facile processing methods, which improve the solubility[21,22] of CNTs without

Received: February 17, 2011
Published: August 10, 2011

Chart 1. Complementary 2,6-Di(acetylamino)pyridine- (1a,b) and Uracil-Bearing (2−4) H-Bonding Monomeric Modules

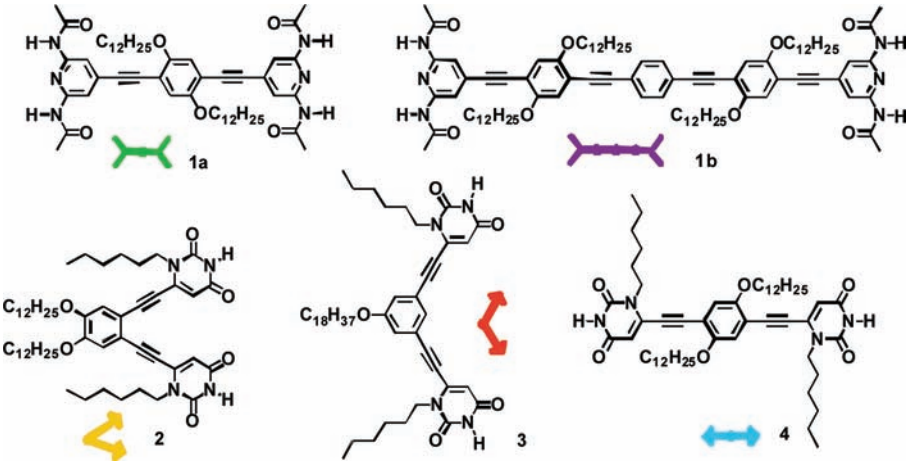

compromising their structural and physical properties, paving the way toward the development of novel CNT-based materials. While the successful solubilization of carbon nanotubes has opened many new perspectives, the ability to tune the functionalization and influence[17,20,21,23] the solubility of the tubes in a controlled way may prove crucial, for example, in complex systems such as smart devices, sensors, or even drug delivery.

Supramolecular polymers,[24,25] constructed by means of noncovalently linked monomeric units, are ideally suited for the manipulation and supramolecular functionalization of CNTs, because they could wrap around the graphitic walls leading to reversible solubilization and precipitation of CNTs through solvent polarity control. The rationale behind this approach is the possibility to exploit the ease of synthesis of the monomeric units, the combination of infinite number of units equipped with specific functionalities, and the predictability of the final targeted assemblies, to obtain well-defined yet flexible systems. Because of their directionality, strength, and versatility, multiple hydrogen bonds have held, by far, a most prominent place in engineering such polymeric arrays.[24,26−28] In addition, their dynamic and combinatorial nature may enable healing and adaptation, and thereby self-organization, by means of secondary weak interactions, such as $\pi-\pi$ and van der Waals.[29] Notwithstanding, the strength of the hydrogen bonds depends mainly on the solvent as well as number and sequence of the H-bond donors and acceptors. By introducing competing solvents, such as polar organic solvents, the H-bonding interactions holding the supramolecular polymers might be broken leading to the monomeric individual units.

To the best of our knowledge, Stoddart et al. have described the first example of a supramolecular polymer interacting with CNTs.[30] Specifically, they have reported the dispersion of single-walled carbon nanotubes (SWCNTs) in aqueous solutions by self-assembling 5,15-bispyridyl Zn(II)-porphyrin complexes. These form charged acyclic and/or cyclic adducts on/or around the sidewalls of SWNTs, by means of dynamic coordinative interactions mediated by *cis* complexes of Pd(II) ions. SWCNTs could also be dissolved in organic solvents through the formation of polymeric mixtures of barbituric acid and triaminopyrimidine scaffolds using mechanochemical high-speed vibration milling (HSVM) under strong sonication conditions.[31]

Under solvent polarity control at mild conditions, herein we report the reversible solubilization and functionalization of multiwalled carbon nanotubes (MWCNTs) through combined self-assembly and self-organization processes mediated by H-bonds. In order to achieve this goal, we have designed and synthesized a library of ditopic molecular modules that expose, at their peripheries, complementary recognition motifs. Exploiting the mimics of complementary base pairing of DNA, a series of molecules featuring 2,6-di(acetylamino)pyridine moieties able to selectively and reversibly recognize uracil-bearing modules have been prepared (Chart 1). The heteromolecular recognition between these units is mediated by triple parallel H-bonds established between the NH−N−NH (DAD = Donor−Acceptor−Donor) functions of the 2,6-di(acetylamino)pyridine and the CO−NH−CO (ADA = Acceptor−Donor−Acceptor) imidic groups of the uracil derivatives. Two types of molecular modules have been prepared: linear modules with the recognition sites positioned at 180° relative to each other (molecules **1a**−**b**, **4**), and angular units (**2**, **3**) with binding residues at 60° or 120°, respectively. Our previous studies have shown that under suitable solvent polarity and temperature control, molecules **1a**/**b** self-assemble and self-organize with complementary modules **2**−**4** to form nanowires.[27,32] The self-assembly and self-organization processes leading to the formation of the supramolecular polymers are driven by the H-bonding interactions between the complementary recognition sites linked to the aromatic units, which are characterized by different geometric constraints. These molecular components undergo self-assembly (Chart 2) in $CHCl_3$, CH_2Cl_2, or toluene and, in the presence of MWCNTs, they self-organize into supramolecular polymers that enfold the external MWCNTs' surface, prompting the solubilization of CNTs. Eventually, addition of polar solvents such as DMSO or MeOH causes the rupture of the H-bonding interactions and, consequently, the partial detachment of the polymer from the carbon frameworks, followed by rapid precipitation of the CNTs. The precipitate is then resolubilized upon solvent removal under vacuum and addition of $CHCl_3$, showing the reversibility of the proposed strategy.

RESULTS AND DISCUSSION

Synthesis. The synthesis of molecular monomeric units **1**−**4** was achieved through Pd(0) cross-coupling reactions by exploiting the protocols already reported in the literature by us.[33,34] Linear module **1a** was prepared via a three-step synthesis starting from 1,4-dihydroquinone (Scheme 1). Alkylation of 1,4-dihydroquinone in 1-bromododecane afforded **6**. Subsequent iodination

by reaction with I_2 in the presence of $Hg(OAc)_2$ as catalyst afforded the diiodinated derivative **7**, which was purified by recrystallization from hot EtOH in a 80% yield. Following this, **7** was cross-coupled with a small excess (2.5 equiv) of 2,6-di(acetylamino)-4-ethynylpyridine[33,34] to obtain **1a**. The compound was purified by column chromatography in SiO_2 (cyclohexane/AcOEt, 1:1). Palladium-catalyzed coupling of the diiodide **7** with trimethylsilylacetylene afforded **11**, which was treated with 1 M aqueous solution of KOH in a MeOH/THF (1:1) mixture, in order to remove the protecting TMS groups. Finally, **4** was obtained under Sonogashira conditions by reacting diacetylene **12** with 1-hexyl-6-iodouracil.[33] Compound **4** was purified by column chromatography (SiO_2, cyclohexane/AcOEt, 7:3→5:5→1:9, finally $CHCl_3$). The structure of all compounds was assessed by EI mass spectrometry, ^1H and ^{13}C NMR, and IR spectroscopies.

The module **1b**, a linear extension of **1a**, is essentially a conjugated phenyleneethynylene oligomer (OPE) terminated with two DAD hydrogen bonding recognition units (Scheme 1). The synthesis of this π-conjugated system was achieved by designing an asymmetrical ethynyl precursor, which allowed selective Pd(0) cross-coupling reaction through a Sonogashira-type reaction. Diiodide derivative **7** was cross-coupled with TMSA (1 equiv) under Sonogashira conditions yielding the monoethynylene **8** in 37% yield. Following this, a second cross-coupling reaction of **8** with 2,6-di(acetylamino)-4-ethynylpyridine[33] afforded the asymmetrically substituted oligophenyleneethynylene **9** in 63% yield, which successfully afforded **10** after treatment with 1 M aqueous solution of KOH in a $MeOH/CH_2Cl_2$ (1:1) mixture. Finally, ethynyl derivative **10** (2.5 equiv) was cross-coupled with 1,4-diiodobenzene affording **1b** (47%). As the reaction proceeds, a yellow fluorescent precipitate started to appear. The mixture was allowed to react overnight, and then the heterogeneous phase was filtered in order to separate the precipitate from the liquid phase. The solution was then concentrated under reduced pressure and the solid purified by column chromatography on silica gel affording **1b**. The structure of the final compound was assessed by ESI−MS, ^1H and ^{13}C NMR, and IR spectroscopies.

Alkylation of 1,2-dihydroquinone with 1-bromododecane in the presence of K_2CO_3 and DMF afforded the bisdodecyloxy benzene **14** that was then iodinated (I_2, $Hg(OAc)_2$) to yield the molecular module **15** (85%), which was purified by recrystallization from hot EtOH (Scheme 2). Cross coupling of **15** with an excess of trimethylsilylacetylene yielded **16**. Removal of TMS groups with 1 M aqueous KOH solution in a 1:1 MeOH/THF mixture gave the terminal bisalkyne **17**. The target compound **2** was finally obtained by coupling of 1-hexyl-6-iodouracil[33] with diacetylene **17** under classical C−C coupling Sonogashira conditions.

Finally, *meta*-ethynyl bis(uracil) **3** was prepared from commercial 3,5-dibromophenol, which was alkylated with iodooctadecane in the presence of K_2CO_3 and DMF to afford **19** (Scheme 3). The exchange of Br_2 by the ethynyl groups at *meta* positions relative to the alkoxy-substituted benzene ring presented some difficulties (Table S1). This could be explained by the fact that aryl bromide **19** is a highly "deactivated" substrate, as it is electron−rich, and therefore the Sonogashira coupling is not so favored and requires high temperatures to proceed. Several catalysts, solvents and temperatures were tested in order to obtain **21** (see Supporting Information, Table S1). In most cases, the coupling reactions proceed just on one Br atom leading

Chart 2. Schematic Representation of the Different Soluble Supramolecular Polymers, $[X•Y]_n$[a]

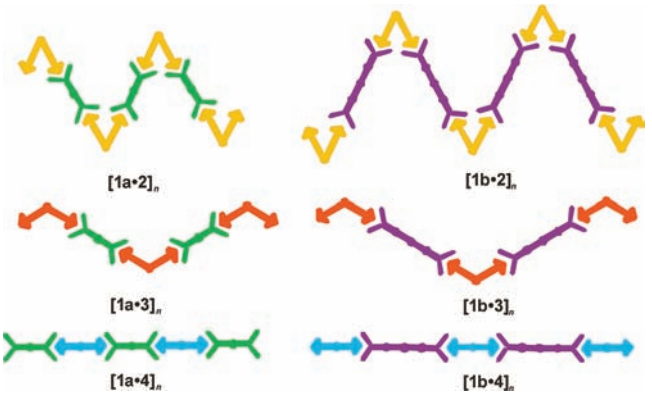

[a]**X** = **1a** or **1b** and **Y** = **2**, **3**, or **4**.

Scheme 1[a]

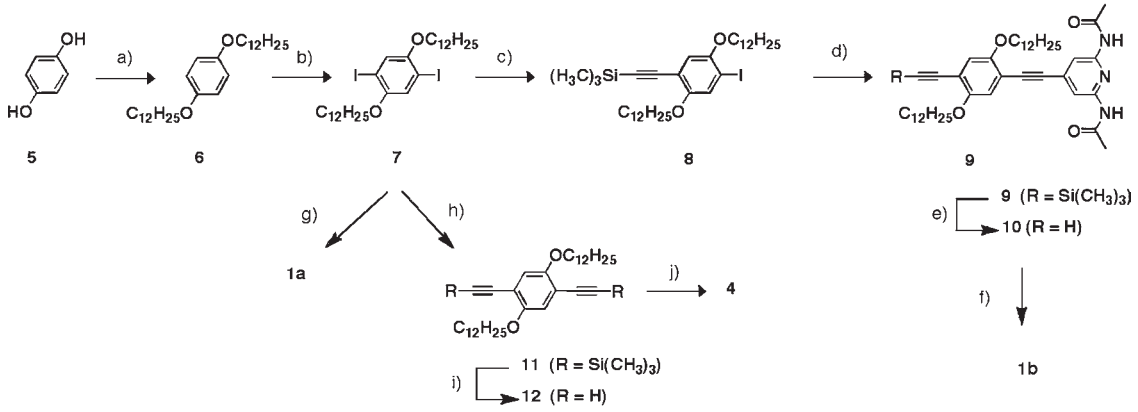

[a] (a) 1-Bromododecane, K_2CO_3, DMF, 60 °C, 12 h, 64%; (b) $Hg(OAc)_2$, I_2, CH_2Cl_2, r.t., 12 h, 80%; (c) TMSA, $[Pd(PPh_3)_4]$, CuI, Et_3N, THF, r.t., 12 h, 37%; (d) 2,6-di(acetylamino)-4-ethynylpyridine[33] $[Pd(PPh_3)_4]$, CuI, Et_3N, THF, r.t., 48 h, 63%; (e) 1 M aq. KOH, $MeOH/CH_2Cl_2$ (1:1), r.t, 1 h, quant.; (f) 1,4-diiodobenzene, $[Pd(PPh_3)_4]$, CuI, Et_3N, THF, r.t., 12 h, 47%; (g) 2,6-di(acetylamino)-4-ethynylpyridine[33] $[Pd(PPh_3)_4]$, CuI, Et_3N, THF, 85 °C, 12 h, 68%; (h) TMSA, $[Pd(PPh_3)_4]$, CuI, Et_3N, THF, r.t., 12 h, 40%; (i) 1 M aq. KOH, MeOH/THF (1:1), r.t, 1 h, quant.; (j) 1-hexyl-6-iodouracil[33] $[Pd(PPh_3)_4]$, CuI, Et_3N, THF, r.t., 12 h, 77%.

Scheme 2[a]

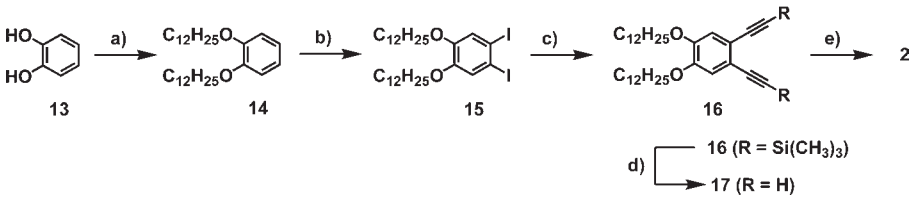

[a] (a) 1-Bromododecane, K_2CO_3, DMF, 60 °C, 12 h, 70%; (b) $Hg(OAc)_2$, I_2, CH_2Cl_2, r.t., 12 h, 85%; (c) TMSA, $[Pd(PPh_3)_4]$, CuI, Et_3N, THF, r.t., 12 h, 36%; (d) 1 M aq. KOH, MeOH, r.t, 1 h, quant.; (e) 1-hexyl-6-iodouracil, $[Pd(PPh_3)_4]$, CuI, Et_3N, THF, r.t., 12 h, 51%.

Scheme 3[a]

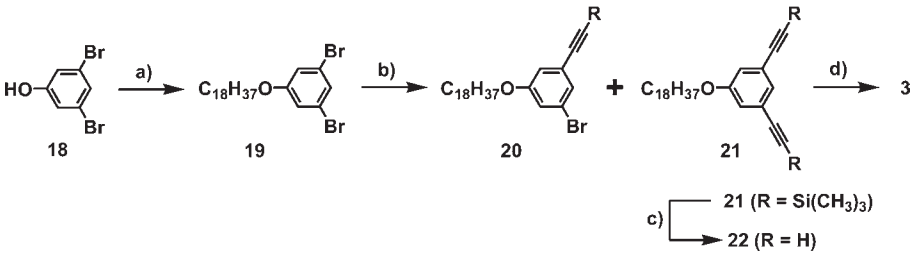

[a] (a) 1-Iodooctadecane, K_2CO_3, DMF, 60 °C, r.t., 12 h, 80%; (b) TMSA, $[PdCl_2(PPh_3)_2]$, CuI, iPr_2NH, DMF, 5 min, 120 °C, MW, 79%; (c) 1 M aq. KOH, MeOH:THF (1:1), r.t., 1 h, quant.; (d) 1-hexyl-6-iodouracil, $[Pd(PPh_3)_4]$, CuI, Et_3N, THF, r.t., 12 h, 46%.

Scheme 4. Schematic Representation of the Supramolecular Functionalization Protocol for the Reversible Solubilization of MWCNTs with Supramolecular Polymers $[X•Y]_n$

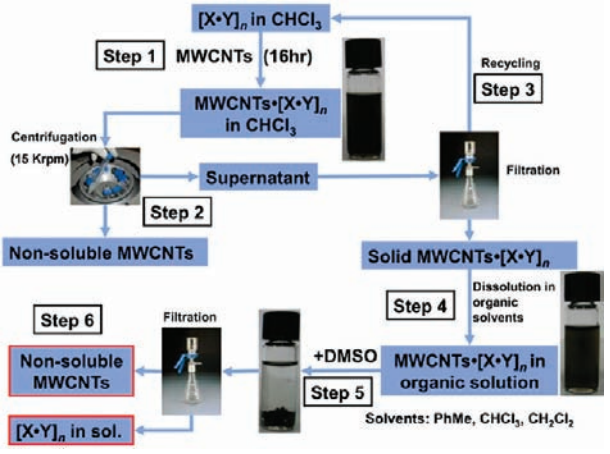

to the mono ethynyl substituted octadecylalkoxybenzene. The best results were obtained when microwave irradiation was applied (entry 5, SI Table S1) which afforded diethynyl-substituted derivative **21** in 79% yield. Targeted compound **3** was finally obtained by cleavage of the TMS in the presence of KOH in a MeOH/THF solution and subsequent C−C coupling with 1-hexyl-6-iodouracil[33] (Scheme 3).

Reversible Solubilization of MWCNTs. The strategy adopted for the reversible solubilization cycle of the MWCNTs is depicted in Schemes 4 and 5. The solution behavior of the hybrid **MWCNTs•[X•Y]$_n$** was monitored both by visual inspection and by using UV−vis spectroscopy. In a classical experiment, a sample of **MWCNTs•[X•Y]$_n$** was prepared by addition of an equimolar solution of the complementary monomeric modules (for example, **1b** and **2** for **MWCNTs•[1b•2]$_n$**, Figure 1c) to a presonicated (sonication bath, room temperature, 3 min) dispersion of pristine MWCNTs (6 mg) in $CHCl_3$ (15 mL) and stirred for 16 h. Interestingly, this procedure resulted in a very stable black solution (Step 1, Scheme 4). The crude solution was further purified by centrifugation at 15 krpm for 30 min (Step 2, Scheme 4) to remove unsolubilized MWCNTs, and the supernatant solution was filtered through a Teflon(JH)Millipore® (0.45 μm) filter and washed with $CHCl_3$ to remove the excess of unbounded molecules. The filtration waters containing the unbound molecules in $CHCl_3$ were concentrated and the molecules recovered were used for the new solubilization cycle to avoid losing the precious molecular modules (i.e., recycling cycle: Step 3, Scheme 4). Quantitative solubilization data from the first cycle (cycle1) and the second solubilization cycle -cycle 2- (i.e., by using the recovered unbounded molecules from cycle 1) are collected in Table 1. The resulting black powder, **MWCNTs•[X•Y]$_n$** hybrid, was dried overnight in vacuum and redissolved (Step 4, Scheme 4) in $CHCl_3$ (or toluene or CH_2Cl_2) leading to very stable (after several months, no precipitation has been observed) dark solutions (Figure 1d). These purified **MWCNTs•[X•Y]$_n$** hybrid solutions were further characterized using various microscopic and spectroscopic techniques (vide infra). The experimentally measured quantities of dissolved hybrids (**MWCNTs•[X•Y]$_n$**) are reported in Table 1. At this stage, we assume that the solubility of **MWCNTs** is induced by intermolecular hydrogen-bonding interactions between the complementary monomeric molecular modules leading to a supramolecular polymer that wraps around CNTs. This proposed mechanism was indirectly confirmed in two ways: (i) ultrasonication and stirring of MWCNTs in the presence of DAD individual molecular modules (i.e., bearing di(acetylamino)pyridine groups, which fail to solubilize individual tubes since they do not form efficient hydrogen bonds) lead to no apparent solubilization (Figure 1b) and (ii) addition of

Scheme 5. Schematic Representation of the Envisaged Self-Assembly and Self-Organization Processes Taking Place in the Presence of the MWCNTs[a]

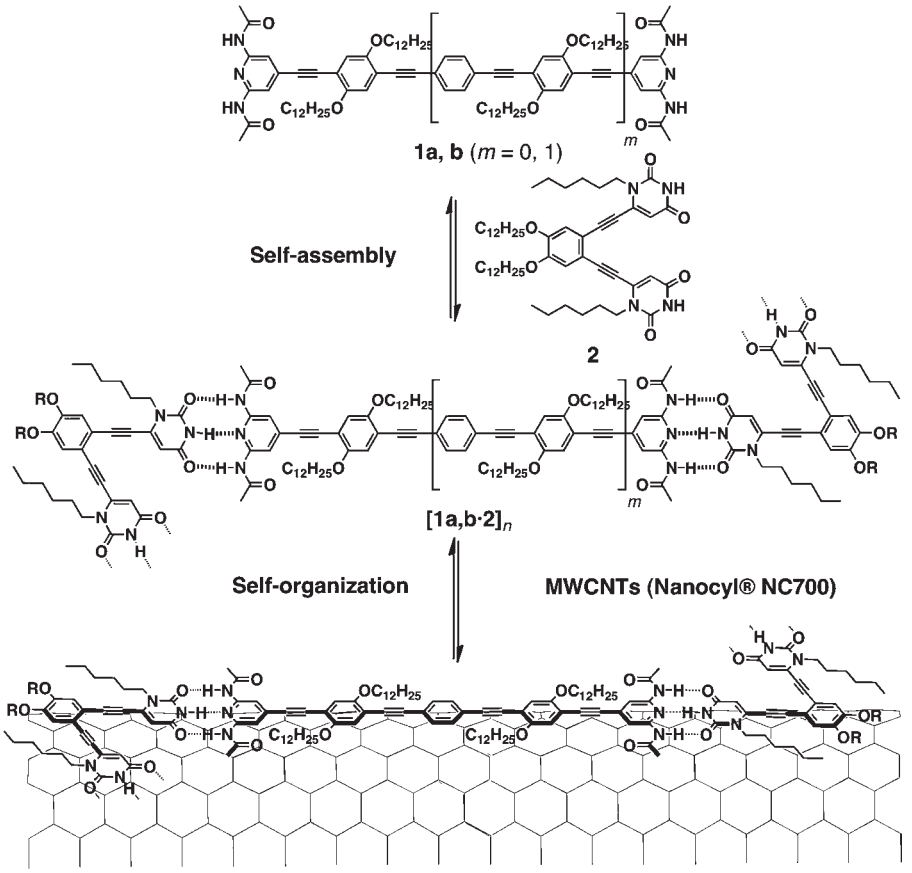

[a] For the sake of clarity, only the examples with the angular module **2** are drawn.

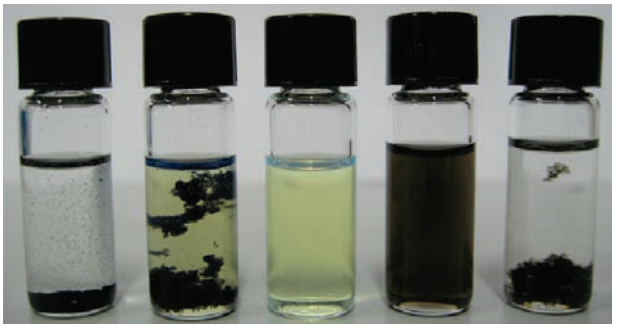

Figure 1. Mixture in $CHCl_3$ containing, from left to right, (a) MWCNTs, (b) MWCNTs and **1b**, (c) polymer $[\mathbf{1b}\bullet\mathbf{2}]_n$, (d) hybrid **MWCNTs**•$[\mathbf{1b}\bullet\mathbf{2}]_n$, and (e) **MWCNTs**, **1b** and **2** after addition of DMSO.

polar solvents like DMSO or MeOH causes immediate precipitation of CNTs (Step 5, Scheme 4, Figure 1e). The spectroscopic investigations carried out on the supernatant solution showed the presence of the constituting molecular units (*vide infra*), thus confirming the polymer detachment from the CNT walls. As a matter of fact, the efficiency of these triple hydrogen bonding interactions is known to decrease considerably in polar solvents like DMSO or MeOH,[35] inducing the disruption of the H-bonded polymeric species and triggering desorption from the MWCNTs and consequent precipitation.

Table 1. Solubilization Experiment: The Quantity Reported Are the weighed CNTs Recovered after a Solubilization/Filtration/Drying Cycle[a]

sample	cycle 1	cycle 2
MWCNTs•$[\mathbf{1b}\bullet\mathbf{2}]_n$	2.72 mg	3.59 mg
MWCNTs•$[\mathbf{1b}\bullet\mathbf{2}]_n$[b]	1.44 mg	2.18 mg
MWCNTs•$[\mathbf{1a}\bullet\mathbf{2}]_n$	0.62 mg	2.21 mg
MWCNTs•$[\mathbf{1a}\bullet\mathbf{4}]_n$	0.35 mg	2.16 mg
MWCNTs•$[\mathbf{1a}\bullet\mathbf{3}]_n$	1.51 mg	–––
MWCNTs•$[\mathbf{4}]_n$	1.15 mg	2.01 mg
MWCNTs•$[\mathbf{2}]_n$	0.92 mg	0.32 mg

[a] For the supramolecular functionalization, 6 mg of MWCNTs were dispersed by sonication in 15 mL of $CHCl_3$ and equimolar quantities (3 mM) of X and Y were added and stirred at rt overnight. [b] In this case, the molecular ratio was 1:2.

^{1}H NMR Studies. In order to prove the dynamic and reversible formation of polymers through complementary H-bonding interactions and their interactions with MWCNTs, a series of ^{1}H NMR experiments were carried out. In a typical experiment, equimolar solutions (ca. 3 mM in $CDCl_3$) of complementary monomeric modules bearing the di(acetylamino)pyridyl units (**1a** or **1b**) and the uracil functionalities (**2** or **3**) were mixed in a NMR tube and allowed to self-assemble for some minutes

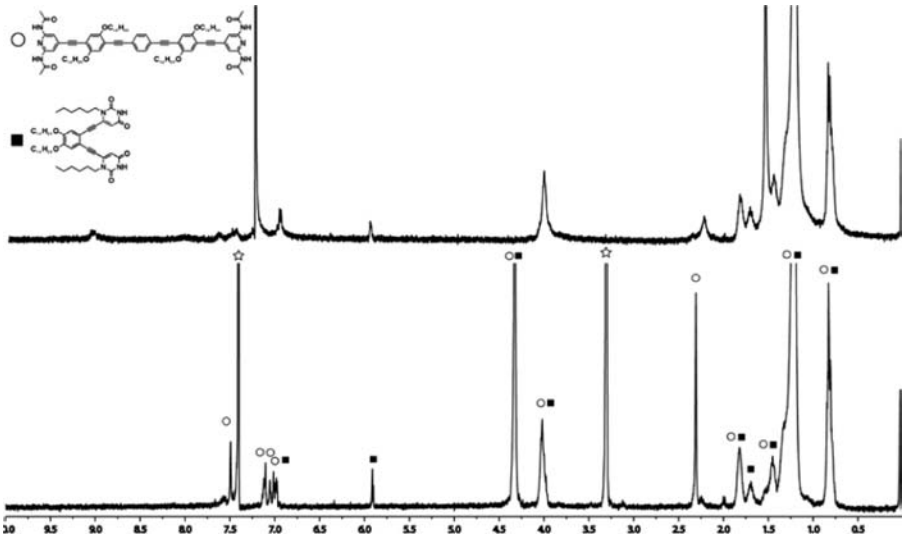

Figure 2. Top: ^{1}H NMR ($CDCl_3$) of $[\mathbf{1b}\bullet\mathbf{2}]_n$ (1:1). Down: ^{1}H NMR ($CDCl_3$+CD_3OD) of $[\mathbf{1b}\bullet\mathbf{2}]_n$ (1:1). ☆ = Solvent residual peaks, ○ = **1b**, ■ = **2**.

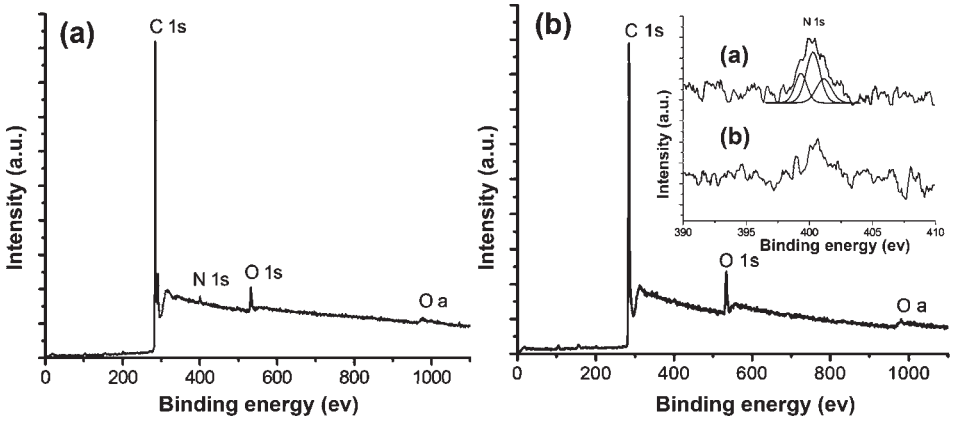

Figure 3. XPS survey spectrum for hybrid **MWCNTs**•$[\mathbf{1b}\bullet\mathbf{2}]_n$ materials (a) before and (b) after washing with DMSO. Inset shows corresponding high-resolution XPS images on N 1s.

before measurements. For example, the ^{1}H NMR spectrum of the solution containing linear unit **1b** and angular module **2** exhibited broad signals (see Figure 2, top) indicating the presence of polymeric-like structures in solution. Furthermore, the signal corresponding to imidic NH protons of molecule **2** underwent a typical downfield shift from 8.4 ppm to ca. 9 ppm of the centered resonances, which confirms the complementary hydrogen bonding interaction between the uracyl and the 2,6-di(acetylamino)pyridine units. These results support the formation of a supramolecular polymer. In fact, when some drops of CD_3OD are added to the $CDCl_3$ solution containing a 1:1 mixture of **1b** and **2**, the spectrum of the initial components is completely recovered (see Figure 2, bottom). In such conditions, all the characteristic signals of both components (except the NH peaks) can be identified. A similar experiment for polymer $[\mathbf{1a}\bullet\mathbf{3}]_n$ can be found in the Supporting Information.

X-ray Photoelectron (XPS) and TGA Analysis. The first evidence for the presence of supramolecular assemblies on the surface of solubilized MWCNTs (**MWCNTs**•$[\mathbf{X}\bullet\mathbf{Y}]_n$) was obtained through XPS analysis. XPS has proven to be a very powerful tool to confirm the presence of non-CNT materials, as it gives information about the atomic compositions and the type of bonds that occur between the atoms. In addition to C 1s (284.7 eV) and O 1s (533.1 eV), XPS spectra of all solubilized MWCNTs exhibit N 1s signal at 400 eV (1.5−1.7%) indicating the presence of supramolecular polymers on the surface of MWCNTs (Figure 3 and Supporting Information). Three nitrogen species must contribute as components to the N 1s peak: two identical pyridyl−N moieties, six and two amide and diimide functions, respectively (the N 1s for the amides of molecules **2** and **1b** have almost the same energy and cannot be resolved in different components). Indeed, we can assign it to photoelectrons emitted from the N atom of pyridines and from the amidic and the diimidic functions; the peaks are centered at 398.5, 400.2, and 401.4 eV, respectively. Interestingly, samples of MWCNTs prepared after washing the hybrid **MWCNTs**•$[\mathbf{X}\bullet\mathbf{Y}]_n$ with DMSO led to spectra displaying a substantial decrease of the peak intensity corresponding to N 1s signal, which confirms the disassembly process. However, a complete disappearance of the N-centered peak of N 1s could not be achieved, showing that tiny traces of physically adsorbed **2** and/or **1b** on the **MWCNTs** are still present on the carbon walls, despite DMSO washing.

The presence of supramolecular polymers $[\mathbf{X}\bullet\mathbf{Y}]_n$ on the surface of MWCNTs was further substantiated through thermogravimetric

dx.doi.org/10.1021/ja2011516 |*J. Am. Chem. Soc.* 2011, 133, 15412–15424

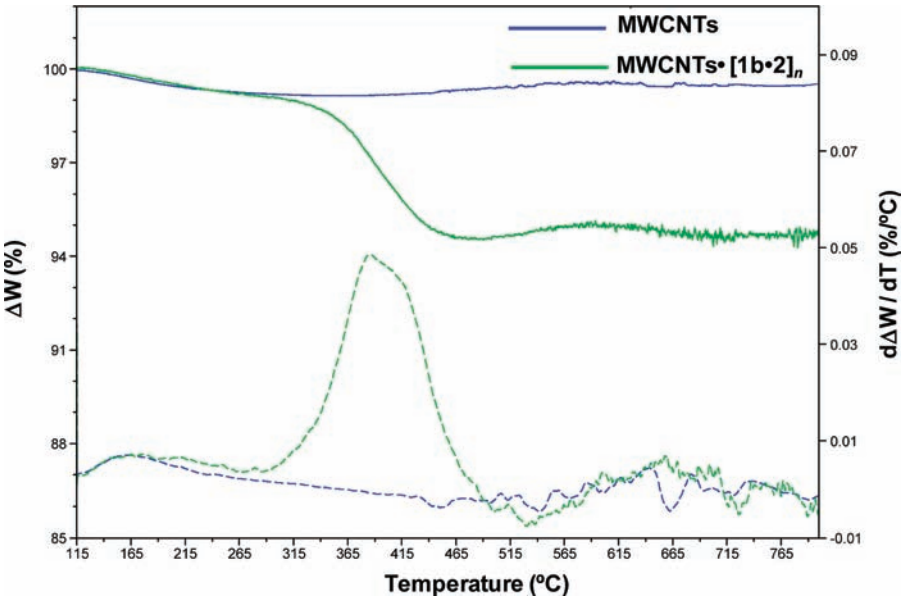

Figure 4. TGA traces (solid line) and their derivatives (dashed line) of pristine **MWCNTs** (blue) and **MWCNTs•**$[\mathbf{1b•2}]_n$ (green). The temperature interval (310−510 °C) represents a steep weight loss due to the degradation of the molecular modules.

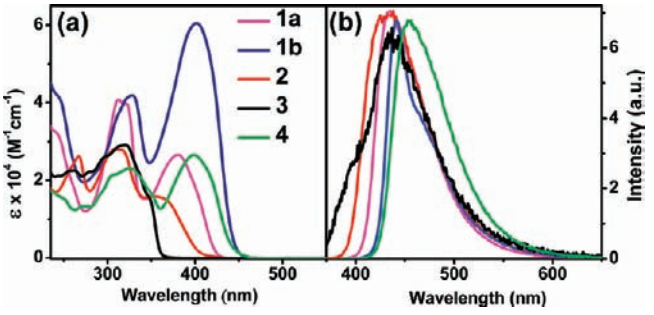

Figure 5. (a) Absorption and (b) fluorescence spectra of **1**−**4** in chloroform. Emission profiles were recorded upon excitation at 308 nm.

(TGA) analysis. As an example, we report the TGA measurements for hybrid **MWCNTs•**$[\mathbf{1b•2}]_n$. A weight loss of 6% (attributed to the polymeric $[\mathbf{1b•2}]_n$ species; see Supporting Information) between the temperatures 310 and 510 °C (Figure 4) has been observed.

Photophysical Investigations: UV−vis−NIR Absorption and Fluorescence Spectroscopies. The absorption and fluorescence spectra of the investigated hydrogen bonding molecular units are depicted in Figure 5, and the related photophysical parameters are summarized in Table 2. Our previous investigations[27,32,36] have shown that molecules **1**−**4** exhibit intense absorption in the UV−visible region and are good luminophores in solution ($CHCl_3$). For example **1a**, **1b**, and **4** exhibit fluorescence quantum yields as high as ∼1, 0.8, and 0.9, respectively, whereas **2** and **3** show weaker quantum yields of ∼0.3 and ∼0.01.

In Figure 6 is summarized an absorption spectral study, in $CHCl_3$, of different combinations of the complementary hydrogen bonding modules **1a**, **1b**, **2**, and **3** compared to the corresponding optically transparent solutions of supramolecularly solubilized **MWCNTs•**$[\mathbf{X•Y}]_n$. (for the absorption spectra of **1a**, **4**, and corresponding **MWCNTs•**$[\mathbf{1a•4}]_n$, see Supporting Information). Equimolar mixtures of the complementary

Table 2. Photophysical Properties in a Chloroform Solution

molecule	$\lambda_{abs.\ max}$ (nm)	$\lambda_{em.\ max}$ (nm)	Φ_{em} (%)	τ_{em} (ns)
1a	312, 380	435	∼100	2.5
1b	330, 398	440	84	1.0
2	305, 354	430	28	1.4
3	320, 350	435	1	2.3
4	325, 400	455	93	1.9

molecules resemble those of their corresponding algebraic sum, except for the combinations of linear linkers **1a** and **1b** with **3**, which exhibit a weak new feature on the lower energy side (420 nm for $[\mathbf{1a•3}]_n$, 460 nm for $[\mathbf{1b•3}]_n$; see the arrows in Figure 6). The presence of this new feature at longer wavelengths is taken as a clue for the formation of supramolecular polymers arising from the combination of H-bond-directed self-assembly and self-organization processes (*vide infra*).[27,28,32,33,36,37] On the contrary, the absorption spectra of solubilized MWCNTs did not reveal any features corresponding to the presence of either of the molecular components. The possible reasons for this observation are (i) overwhelming absorption of CNTs, (ii) supramolecular organization of molecules into new materials which perturbs their initial spectra, or (iii) a combination of these effects. More interestingly, in the case of MWCNTs solubilized using **1b** with a combination of either **2** or **3**, we observed a weak band at the longer wavelengths (see the encircled areas in Figure 6). For example, the **MWCNTs•**$[\mathbf{1b•2}]_n$ exhibits a shoulder at 490 nm and **MWCNTs•**$[\mathbf{1b•3}]_n$ have weak absorption at 455 nm. In other cases, **MWCNTs•**$[\mathbf{1a•2}]_n$ and **MWCNTs•**$[\mathbf{1a•3}]_n$, the new features are hardly visible. The origin of this new absorption feature is attributed to the presence of supramolecular polymeric materials on the surface of MWCNTs (*vide infra*).[27,32,33,36,37]

In parallel to the absorption spectral measurements, we investigated the emission properties of the **MWCNTs•**$[\mathbf{X•Y}]_n$ materials. None of the solubilized **MWCNTs•**$[\mathbf{X•Y}]_n$ materials showed significant emission signals. As an example, the fluorescence

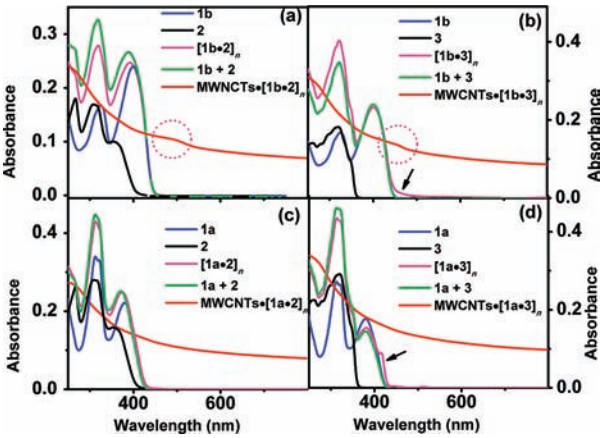

Figure 6. Absorption spectra in $CHCl_3$ of isolated molecular subunits (**1**−**3**, blue and black) and their combinations with (red) and without MWCNTs (magenta). Green lines correspond to algebraic summation of spectra.

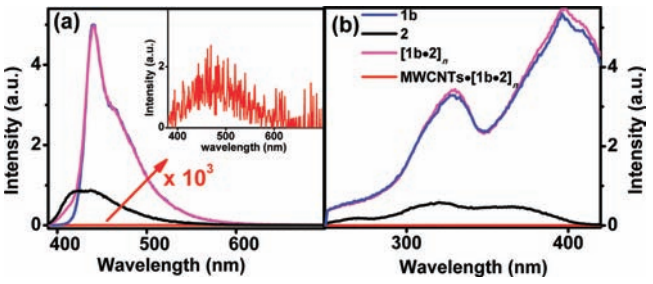

Figure 7. (a) Emission and (b) excitation spectra in $CHCl_3$ of **1b** (blue), **2** (black), $[\mathbf{1b•2}]_n$ (magenta), and **MWCNTs•**$[\mathbf{1b•2}]_n$ (red). Inset: residual emission from **MWCNTs•**$[\mathbf{1b•2}]_n$: emission spectra were collected upon excitation at 360 nm; excitation spectra were recorded at the respective emission maximum.

spectra of **1b**, **2**, their equimolar mixture ($[\mathbf{1b•2}]_n$), and an optically transparent solution of **MWCNTs•**$[\mathbf{1b•2}]_n$ in $CHCl_3$ are reported in Figure 7. The solutions were excited at 360 nm where the two molecules, **1b** and **2**, exhibit the same absorbance at the used concentration (3.3×10^{-6} M in $CHCl_3$). The largely predominant luminescence signal in $[\mathbf{1b•2}]_n$ stems from molecule **1b** because it exhibits a higher fluorescence quantum yield (84%) compared to angular module **2** (28%), and this is confirmed by the excitation spectrum, which matches that of **1b** (Figure 7b).

On the contrary, under identical conditions, **MWCNTs•**$[\mathbf{1b•2}]_n$ did not show any significant fluorescence; the residual signal, shown in the inset of Figure 7a, arises from the presence of traces of unbound molecules in solution, as confirmed by lifetime measurements (τ = 1 ns). In principle, this observation could be due to the virtual absence of molecules in solution or to the fluorescence quenching of the fluorophores through energy transfer to the low-lying states of MWCNTs. The former explanation is ruled out by further manipulation of the sample. Addition of DMSO (1:3 v/v), followed by filtration of the resulting precipitated MWCNTs, leads to a solution exhibiting a neat fluorescence band fully superimposable in shape to that of $[\mathbf{1b+2}]_n$, with related absorption features (Figure 8). It has to be noted that the differences in the absorption features at shorter wavelengths are due to the presence of DMSO and nonprecipitated CNTs. Notably, upon addition of DMSO, the feature

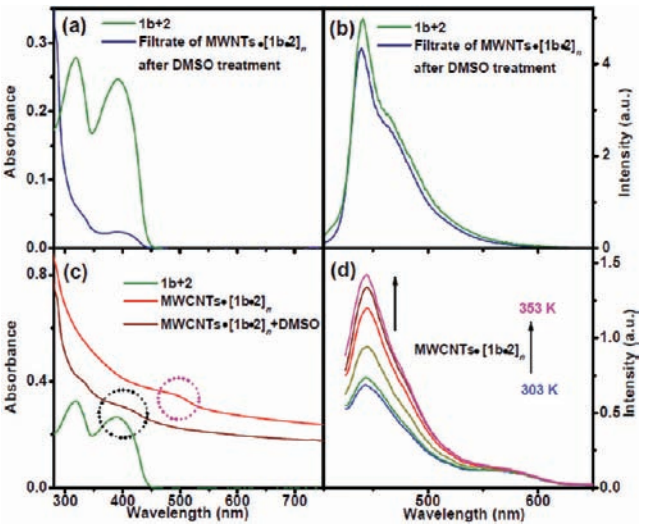

Figure 8. (a) Absorption and (b) emission spectra of $[\mathbf{1b•2}]_n$ (green) and the filtrate of **MWCNTs•**$[\mathbf{1b•2}]_n$ (blue) after DMSO treatment. (c) Comparison of absorption spectra of $[\mathbf{1b•2}]_n$ (green), **MWCNTs•**$[\mathbf{1b•2}]_n$ (red), and **MWCNTs•**$[\mathbf{1b•2}]_n$ in the presence of DMSO (brown). (d) Emission spectral changes of **MWCNTs•**$[\mathbf{1b•2}]_n$ as a function of temperature.

observed at 490 nm for a solution of **MWCNTs•**$[\mathbf{1b•2}]_n$ in $CHCl_3$ got blue-shifted to 400 nm (before the filtration of MWCNTs, see encircled regions in Figure 8c). Our previous investigations have shown that in nonpolar solvents like cyclohexane and toluene a 1:1 mixture of molecular modules bearing complementary H-bonding functionalities at both ends undergo self-assembly and self-organization leading to the formation of nanowires, which exhibit red-shifted absorption features due to $\pi-\pi$ interactions. The new band observed at 490 nm for **MWCNTs•**$[\mathbf{1b•2}]_n$ is thus attributed to the supramolecular $[\mathbf{1b•2}]_n$ polymer species on the surface of MWCNTs. This assumption is corroborated by the spectral studies performed as a function of temperature. In fact, an increase of temperature is expected to cause the disassembly of supramolecular polymers and the detachment of molecules from the surface of nanotubes,[27,32] with suppression of energy transfer from molecules to MWCNTs. Absorption spectral studies performed as a function of temperature did not provide reliable data due to lack of optical transparency, following the formation of large CNT aggregates at higher temperatures. On the contrary, fluorescence spectra recorded in the 303−305 K range show a more than 2-fold increase of the $[\mathbf{1b•2}]_n$-centered fluorescence intensity (Figure 8d).

Further proof of the reversibility of polymer (see also Scheme 5) wrapping onto the CNTs is displayed in Figure 9. Upon addition of MeOH (2:1 v/v) into a solution of **MWCNTs•**$[\mathbf{1b•2}]_n$ in $CHCl_3$, precipitation of MWCNTs was observed as a consequence of the disruption of the hydrogen-bonding interactions (see the particles in sample b, Figure 9a). Complete removal of the solvent through *in vacuo* evaporation left the sample at the bottom of the flask as a black precipitate. Redispersion of the black precipitate in $CHCl_3$ under mild sonication led again to an optically neat solution (sample d in Figure 9a). The normalized absorption spectra of **MWCNTs•**$[\mathbf{1b•2}]_n$ before and after MeOH treatment in $CHCl_3$ (Figure 9b) largely exhibit the same spectroscopic features, indicating the reversibility of the self-assembly and self-organization processes.

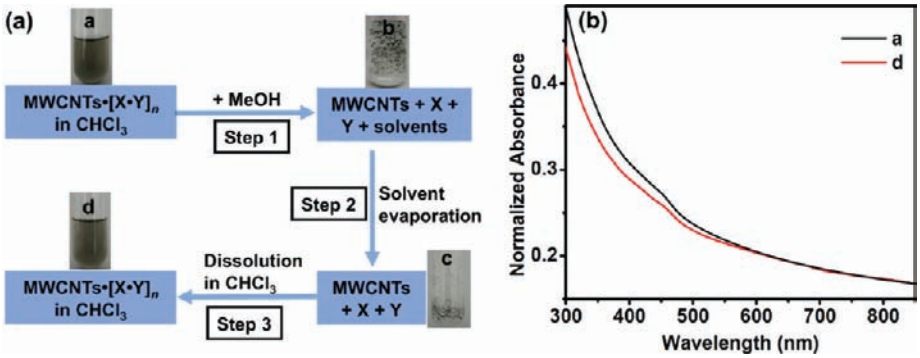

Figure 9. (a) Photographs showing visual changes under MeOH treatment and resolublization of **MWCNTs•[1b•2]**$_n$ in $CHCl_3$. (b) Normalized absorption spectra in chloroform of **MWCNTs•[1b•2]**$_n$ before MeOH treatment (a, black curve) and redissolved in $CHCl_3$ after MeOH addition (d, red curve); absorption spectra were normalized at 850 nm.

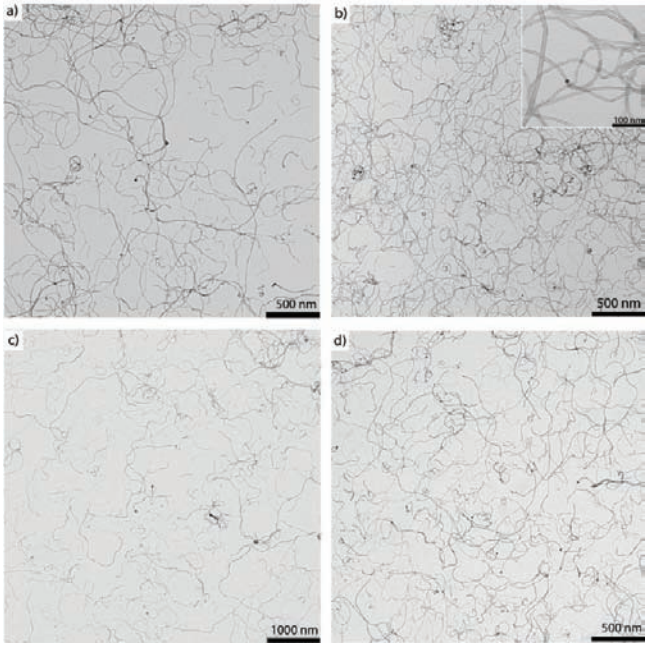

Figure 10. LR−TEM image of (a) hybrid **MWCNTs•[1a•2]**$_n$, (b) hybrid **MWCNTs•[1b•2]**$_n$, (c) hybrid **MWCNTs•[1a•3]**$_n$, and (d) hybrid **MWCNTs•[1a•4]**$_n$ deposited on carbon grids.

Microscopic Analysis (TEM, AFM, and STM). To probe the presence of the **MWCNTs•[X•Y]**$_n$ hybrids and to assess the homogeneity and purity of the samples, microscopy studies were carried out. TEM analysis was made with all hybrids (**MWCNTs•[X•Y]**$_n$, **X** = **1a** or **1b**, and **Y** = **2**, **3** or **4**) as depicted in Figure 10. Samples were prepared by drop-casting the corresponding solution of **MWCNTs•[X•Y]**$_n$ in $CHCl_3$ onto a carbon grid. After treatment of the raw MWCNTs with the different supramolecular polymers and removal of the nonsolubilized tubes, the analysis of the solution phase displayed in all cases a homogeneous distribution of MWCNTs. No remarkable differences were observed among the different soluble hybrid **MWCNTs•[X•Y]**$_n$ systems, showing the versatility in terms of solubility of the molecular library presented here. With regard to the purity, we found minor differences with respect to the pristine material, indicating a high level of purity of the starting sample of MWCNTs.

To further substantiate the attachment of supramolecular polymers on the surface of MWCNTs, AFM/STM investigations were performed. AFM samples were prepared by drop-casting ~20 μL of the corresponding solubilized **MWCNTs•[X•Y]**$_n$ onto a freshly cleaved mica surface. The samples were air-dried and imaged with an AFM apparatus in the tapping mode. Typical AFM images of solubilized MWCNTs using different molecular combinations are presented in Figure 11. The large-scale images recorded from different areas of the samples indicated the presence of well-separated MWCNTs. A closer analysis of these samples by real-time zoom clearly showed the presence of periodic structures having alternating lumps on MWCNTs. The distance between either two adjacent heights or depths ranges from 50 to 100 nm. These periodic structures are attributed to the supramolecular hydrogen-bonded polymeric nanowires that efficiently wrap around MWCNTs (see also Scheme 5), thus imparting solubility.

The morphological properties of the **MWCNTs•[X•Y]**$_n$ hybrids have been also investigated by means of STM under UHV conditions (see **MWCNTs•[1a•2]**$_n$ as an example in Figure 12) after spin-coating of a $CHCl_3$ solution onto a Au/mica substrate (see experimental section in Supporting Information for details). Due to the convolution of the tip shape with the surface topography, the measure of a **MWCNTs•[1a•2]**$_n$ diameter by STM must be extracted from the height of the **MWCNTs•[1a•2]**$_n$, rather than their apparent width. The diameter of the **MWCNTs•[1a•2]**$_n$ ranges from 8 to 18 nm. The reason for spreading of the **MWCNTs•[1a•2]**$_n$ height measurement is attributed to the wrapping of polymer [**1a•2**]$_n$. The most striking characteristic observed in the images is the presence of bright periodic lumps (Figure 12b,c) on the outer surface of all analyzed **MWCNTs•[1a•2]**$_n$ hybrids, that we tentatively attribute to the organic functions of the wrapped polymeric structure (such bright lumps were absent on the pristine MWCNTs). The corrugation (respectively periodicity) of the pattern is approximately 9 nm (respectively 50 nm). While the measured corrugation height (9 nm) suggests another level (vertical) of organization which could stem from the formation of fiber-like structures (the structure of which is difficult to interpret at this stage due to the large size of the system that could not be theoretically modeled), the longitudinal (~50 nm) periodicity nicely fits the pitch values extrapolated from the computationally modeled CNT−polymer hybrids.

Theoretical Simulations. The proposed model of an H-bonded polymer formed by self-assembly of 2,6-di(acetylamino)pyridyl and uracyl moieties at the polymer/CNT interface has been studied with molecular dynamics calculations to obtain further insight into the

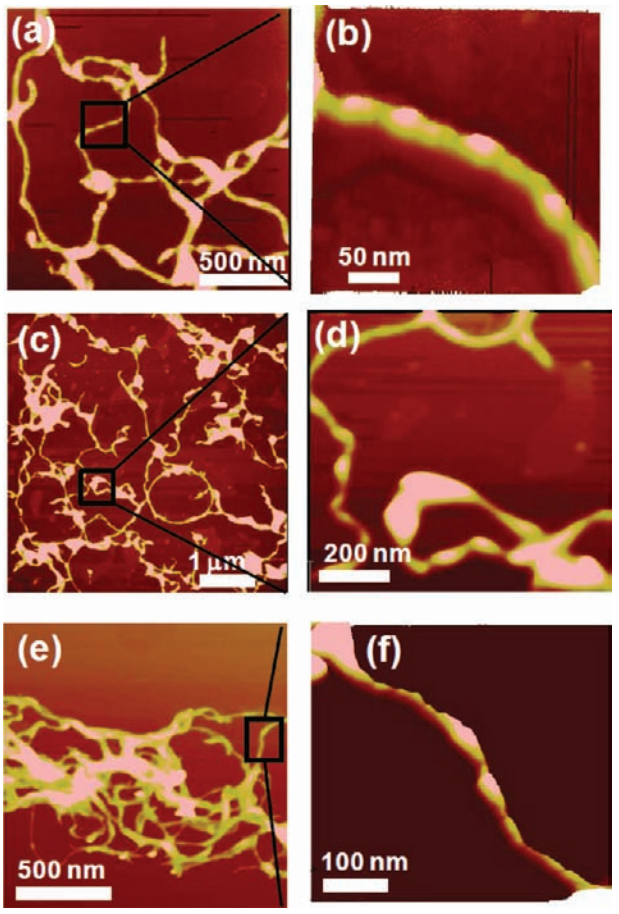

Figure 11. Topographic TM—AFM images of (a) **MWCNTs•[1a•3]**$_n$, (c) **MWCNTs•[1b•2]**$_n$, and (e) **MWCNTs•[1b•3]**$_n$ as deposited by spin-coating a $CHCl_3$ solution on freshly cleaved mica surfaces. Images (b), (d), and (f) represent the zoomed 3D images clearly showing periodic structures of helical wrapping on the MWCNT (images (b) and (f) are rotated by 90° for clarity reasons).

MWCNTs•[X•Y]$_n$ structure (see also Scheme 5) and to elucidate its exceptional solubility. The components are expected to interact in a way that maximizes the number of H-bonds; this criterion can, in principle, be satisfied by the three different molecular organizations schematized in Figure 13.

The closed assembly of Figure 13a does not lead to the formation of an H-bonded polymer, and is less stable, due to steric hindrance generated by the aliphatic chains. Open assemblies such as those in Figure 13b and c are stable and can lead to the formation of H-bonded polymer chains. We have thus focused our attention on the modeling of the structure displayed in Figure 13c, which leads to the formation a regular "zig-zag" polymer. To reduce the computational costs of the modeling, we did not include the solvent in the simulations and we considered a frozen (77,77) SWNT (diameter of 10.5 nm) in order to model the external wall of a typical MWCNT; the freezing of the atomic positions in the nanotube is justified by the fact that the physisorption of the polymer chains is not expected to modify the structure of the carbon wall. The considered CNT model is periodic, in order to avoid edge effects, and an orthorhombic simulation box of about 25 × 20 × 25 nm^3 is used. The box can accommodate five 2,6-di(acetylamino)pyridyl and four uracyl molecules in a zig-zag fashion (Figure 13c), as shown in Figure 14.

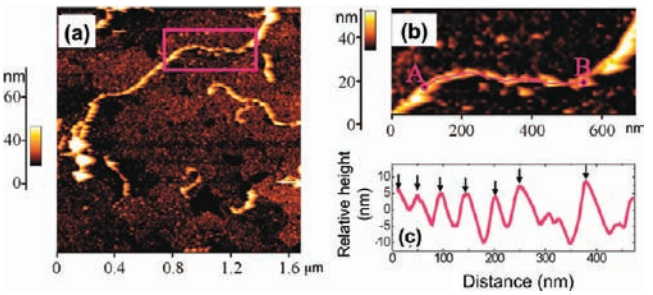

Figure 12. STM image of (a) **MWCNTs•[1a•2]**$_n$ spin-coated onto Au(111)/mica surface; (b) zoomed area showing the presence of periodic lumps on the **MWCNTs•[1a•2]**$_n$ hybrids; (c) height profile along the line A to B, clearly displaying the periodic height oscillation that derives from the helical wrapping of the polymer around a MWCNT (cfr with AFM images in Figure 11).

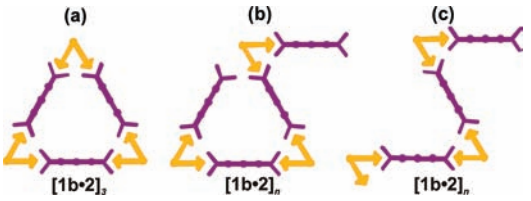

Figure 13. Schemes of the three molecular arrangements that maximize the number of intermolecular H-bonds. (a) is a closed assembly, i.e., not suitable for the formation of H-bonded polymer chains. Furthermore, steric hindrance destabilizes such supramolecular organization. (b) leads to a more disordered polymer, while (c) shows the formation of a regular H-bonded "zig-zag" polymer.

Figure 14 also contains a side view (i.e., along the main axis of the nanotube) of the system, to show that the molecules are completely adsorbed on the carbon nanotube, and can adapt to its curvature. The molecular dynamics (MD) simulations have been performed at room temperature using the molecular modeling code GROMACS and the OPLS-AA force field.

Simulations show that the proposed assembly is rather stable on the CNT surface: it neither breaks up nor presents strong deformations even after several nanoseconds of simulation (see Figure 15). At the end of a 5-ns-long MD trajectory, the zig-zag assembly remains intact; it has simply rotated on the surface to form an angle with the main axis of the nanotube (indicated by the black arrow in Figure 15). In the starting configuration, the axis of all the phenylethynylene moieties is tilted at about 45° with respect to the axis of the tube. Those moieties inherently tend to be straight and flat, and such tilting forces them to bend and follow the nanotube surface. In the final configuration, because of the rotation of the assembly, part of the phenylethynylene units are parallel to the tube axis and do not have to bend to adsorb, while other units are more tilted. It thus seems that such mixing of more favorable and less favorable tilting is more stable than the system in which all units are tilted with respect to the tube axis and bent. The complementary molecular modules are still bonded together via H-bonds after the dynamic optimization. A detailed analysis of the MD trajectory shows that at least one H-bond is always present between two complementary units whereas the others are continuously formed and broken, revealing a great dynamic nature.

In order to evaluate the stability of the assembly, we compared the energies of the H-bonded polymer with those of the isolated

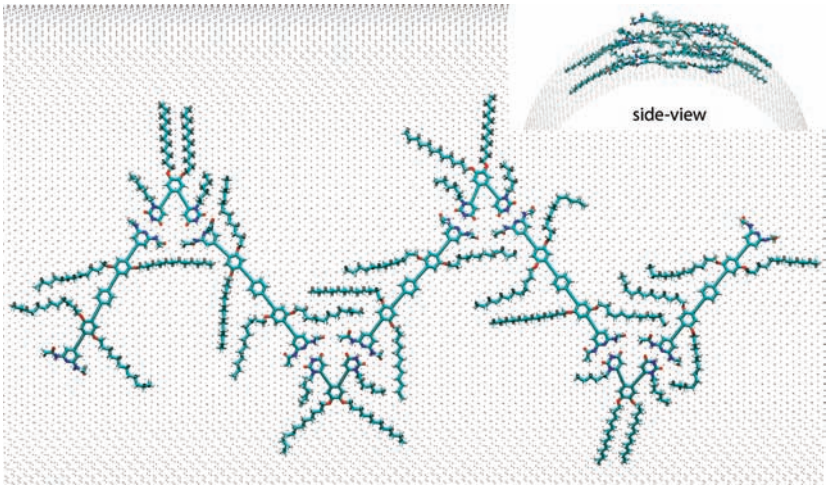

Figure 14. Optimized geometry used as starting points for the MD simulations. The atoms in the nanotube have been dotted to highlight the molecular assembly. The molecules are linked together via H-bonds as in Figure 13c. The polymer is oriented along the main axis of the nanotube; the side view (inset on the upper part) highlights the fact that the molecules are fully adsorbed on the nanotube, adapting to its curvature.

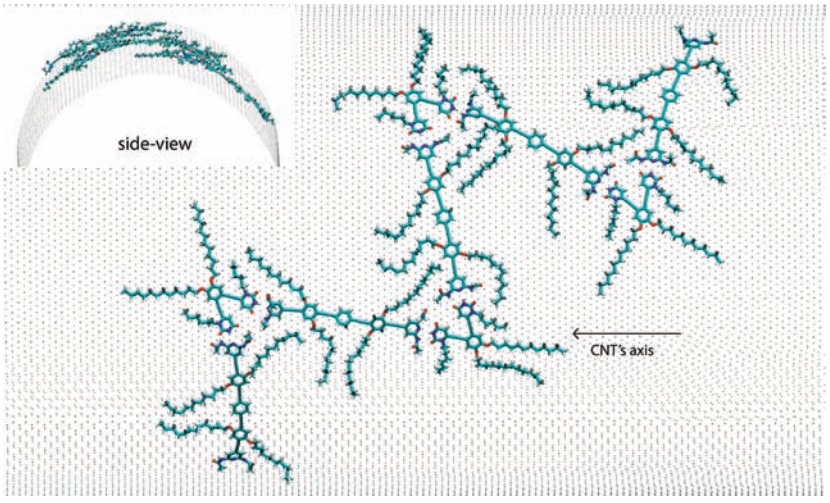

Figure 15. The "zig-zag" disposition of the polymer at the end of a 5-ns-long MD simulation. The complementary molecular modules are still dynamically bonded via H-bonds. The polymer has rotated to form an angle with the axis of the nanotube (black arrow).

molecules in vacuo, using the equation below (where $E^{vac}_{pyridyl}$ and E^{vac}_{uracyl} are the potential energies of isolated pyridyl and uracyl units, N_1 and N_2 are the number of pyridyl and uracyl units, and $E_{polymer}$ is the potential energy of the polymer. E is the stabilization energy resulting from the formation of the polymer, scaled to the number of monomeric units)

$$E = \frac{E_{polymer} - (N_1 \cdot E^{vac}_{pyridyl} + N_2 \cdot E^{vac}_{uracyl})}{N_1 + N_2}$$

Upon formation of the supramolecular polymer $[\mathbf{X}\bullet\mathbf{Y}]_n$ structure and its adsorption on the nanotube surface, two energetic aspects have to be considered as a consequence of the conformational geometry that the molecules have to adopt to adsorb on the CNT. First, the geometrical reorganization of the molecular structure into a flattened conformation adsorbed on the CNT wall torsionally stresses the degrees of freedom of the decorating aliphatic chains and induces a steric repulsion between some of the alkyl groups; this costs, on average, 450 kJ mol^{-1}. Nevertheless, this energy loss is largely compensated by the favorable van der Waals interactions between the polymer molecular modules and the CNT surface ($\pi-\pi$ interactions with the aromatic units and CH$-\pi$ with the alkyl groups). As a result, adsorption leads to a global average stabilization energy of 192 kJ mol^{-1} with respect to the isolated systems. These results support the proposed model of the formation of a stable H-bonded polymer that strongly adsorbs on the surface of carbon nanotubes.

CONCLUSIONS

Although considerable progress has already been made to find new ways to disperse, separate, and purify CNTs, their noncovalent functionalization is still under vigorous development. Conceptually, the research described in this work introduces the idea of using H-bonded polymers to carry out a reversible supramolecular derivatization of MWCNTs, exploiting the dynamic

noncovalent character of weak triple H-bonding interactions such as those established between complementary uracil and 2,6-di(acetylamino)pyridyl recognition moieties. In particular, oligophenyleneethynylene molecular modules laterally equipped with solubilizing aliphatic chains and peripherally bearing two complementary hydrogen-bonding recognition units at their extremities promote a self-assembly process generating supramolecular polymers that self-organize on the CNT surfaces in nonpolar organic media and disassemble upon addition of polar H-bond-breaking solvents (e.g., MeOH or DMSO). Unambiguous proofs of the formation of **MWCNTs•[X•Y]$_n$** hybrids, independent of their structure or geometry, have been provided by several spectroscopic (absorption, emission, XPS), thermogravimetric (TGA) and microscopic (TEM, AFM, STM) techniques. Also, molecular modeling has been used to shed further light on the self-organization process occurring between the supramolecular polymers and the MWCNTs. In fact, if properly functionalized, the supramolecular polymers introduced here can be regarded as an alternative strategy to introduce desired functionalities onto the CNT framework leaving unaltered its structural, chemical, and physical properties. The methodology presented in this manuscript is thus generic and can be extended to other systems of interest opening up new avenues toward the use of these carbon nanostructures in novel applications, such as purification and separation of CNTs.

■ ASSOCIATED CONTENT

Supporting Information. Detailed synthesis of molecular modules and all experimental part. ^{1}H and ^{13}C NMR spectra. XPS and TGA analysis of hybrids. Photophysical investigations. TEM and AFM of MWCNTs hybrids. This material is available free of charge via the Internet at http://pubs.acs.org.

■ AUTHOR INFORMATION

Corresponding Author

Roberto.Lazzaroni@umons.ac.be; nicola.armaroli@isof.cnr.it; davide.bonifazi@fundp.ac.be

■ ACKNOWLEDGMENT

This work was supported by the European Union through the Marie Curie Initial Training Network "FINELUMEN" (grant agreement PITN−GA−2008−215399). D.B. and R.L. especially acknowledge the Belgian National Research Foundation (FRS−FNRS, through the contracts no 2.4.625.08 F, F.4.505.10. F, and 2.4.617.07.F), the "Loterie Nationale", and the Région Wallonne through the "SOLWATT" program (contract no 850551). D.B. also thanks the "TINTIN" ARC project from the Belgian French Community (contract no 09/14−023), the University of Trieste, INSTM, and the University of Namur for internal funding. N.A. thanks CNR (commessa PM.P04.010, MACOL) and H.T. FRS−FNRS for his postdoctoral fellowship. We are also grateful to Nanocyl for supplying the Nanocyl 7000 samples.

■ REFERENCES

(1) Iijima, S. *Nature* **1991**, *354*, 56.
(2) Terrones, M. *Int. Mater. Rev.* **2004**, *49*, 325.
(3) Lu, W.; Lieber, C. M. *Nat. Mater.* **2007**, *6*, 841.
(4) Kreupl, F. *Carbon Nanotubes in Microelectronic Applications*; Wiley-VCH: Weinheim, 2008.
(5) Avouris, P.; Freitag, M.; Perebeinos, V. *Nat. Photonics* **2008**, *2*, 341.
(6) Bottari, G.; de la Torre, G.; Guldi, D. M.; Torres, T. *Chem. Rev.* **2010**, *110*, 6768. Sgobba, V.; Guldi, D. M. *Chem. Soc. Rev.* **2009**, *38*, 165.
(7) Lim, K. L.; Kazemian, H.; Yaakob, Z.; Daud, W. R. W. *Chem. Eng. Technol.* **2010**, *33*, 213.
(8) Kong, J.; Franklin, N. R.; Zhou, C. W.; Chapline, M. G.; Peng, S.; Cho, K. J.; Dai, H. J. *Science* **2000**, *287*, 622.
(9) Rahman, G. M. A.; Troeger, A.; Sgobba, V.; Guldi, D. M.; Jux, N.; Balbino, D.; Tchoul, M. N.; Ford, W. T.; Mateo-Alonso, A.; Prato, M. *Chem.—Eur. J.* **2008**, *14*, 8837.
(10) Kauffman, D. R.; Star, A. *Chem. Soc. Rev.* **2008**, *37*, 1197.
(11) Kostarelos, K.; Bianco, A.; Prato, M. *Nat. Nanotechnol.* **2009**, *4*, 627. Bianco, A.; Kostarelos, K.; Prato, M. *Expert Opin. Drug Delivery* **2008**, *5*, 331. Prato, M.; Kostarelos, K.; Bianco, A. *Acc. Chem. Res.* **2008**, *41*, 60. Saito, N.; Usui, Y.; Aoki, K.; Narita, N.; Shimizu, M.; Hara, K.; Ogiwara, N.; Nakamura, K.; Ishigaki, N.; Kato, H.; Taruta, S.; Endo, M. *Chem. Soc. Rev.* **2009**, *38*, 1897.
(12) D'Souza, F.; Ito, O. *Chem. Commun.* **2009**, 4913. Georgakilas, V.; Bourlinos, A.; Gournis, D.; Tsoufis, T.; Trapalis, C.; Mateo-Alonso, A.; Prato, M. *J. Am. Chem. Soc.* **2008**, *130*, 8733.
(13) Singh, P.; Campidelli, S.; Giordani, S.; Bonifazi, D.; Bianco, A.; Prato, M. *Chem. Soc. Rev.* **2009**, *38*, 2214.
(14) Perez, E. M.; Illescas, B. M.; Herranz, M. A.; Martin, N. *New J. Chem.* **2009**, *33*, 228. Yu, M.; Zu, S.-Z.; Chen, Y.; Liu, Y.-P.; Han, B.-H.; Liu, Y. *Chem.—Eur. J.* **2010**, *16*, 1168. Mateo-Alonso, A.; Ehli, C.; Chen, K. H.; Guldi, D. M.; Prato, M. *J. Phys. Chem. A* **2007**, *111*, 12669. Liu, J.; Bibari, O.; Mailley, P.; Dijon, J.; Rouviere, E.; Sauter-Starace, F.; Caillat, P.; Vinet, F.; Marchand, G. *New J. Chem.* **2009**, *33*, 1017. Zu, S.-Z.; Sun, X.-X.; Liu, Y.; Han, B.-H. *Chem. Asian J.* **2009**, *4*, 1562.
(15) Star, A.; Stoddart, J. F.; Steuerman, D.; Diehl, M.; Boukai, A.; Wong, E. W.; Yang, X.; Chung, S.-W.; Choi, H.; Heath, J. R. *Angew. Chem., Int. Ed.* **2001**, *40*, 1721. Kang, Y. K.; Lee, O.-S.; Deria, P.; Kim, S. H.; Park, T.-H.; Bonnell, D. A.; Saven, J. G.; Therien, M. J. *Nano Lett.* **2009**, *9*, 1414. Zheng, M.; Jagota, A.; Semke, E. D.; Diner, B. A.; Mclean, R. S.; Lustig, S. R.; Richardson, R. E.; Tassi, N. G. *Nat. Mater.* **2003**, *2*, 338. Chen, J.; Liu, H.; Weimer, W. A.; Halls, M. D.; Waldeck, D. H.; Walker, G. C. *J. Am. Chem. Soc.* **2002**, *124*, 9034. Srinivasan, S.; Babu, S. S.; Praveen, V. K.; Ajayaghosh, A. *Angew. Chem., Int. Ed.* **2008**, *47*, 5746. Park, S.; Yang, H.-S.; Kim, D.; Jo, K.; Jon, S. *Chem. Commun.* **2008**, 2876. Curran, S. A.; Ajayan, P. M.; Blau, W. J.; Carroll, D. L.; Coleman, J. N.; Dalton, A. B.; Davey, A. P.; Drury, A.; McCarthy, B.; Maier, S.; Strevens, A. *Adv. Mater.* **1998**, *10*, 1091. Hellstrom, S. L.; Lee, H. W.; Bao, Z. *ACS Nano* **2009**, *3*, 1423. Lee, H. W.; You, W.; Barman, S.; Hellstrom, S.; LeMieux, M. C.; Oh, J. H.; Liu, S.; Fujiwara, T.; Wang, W. M.; Chen, B.; Jin, Y. W.; Kim, J. M.; Bao, Z *Small* **2009**, *5*, 1019. Geng, J.; Zeng, T. *J. Am. Chem. Soc.* **2006**, *128*, 16827. Gu, H.; Swager, T. M. *Adv. Mater.* **2008**, *20*, 4433. Ago, H.; Petritsch, K.; Shaffer, M. S. P.; Windle, A. H; Friend, R. H. *Adv. Mater.* **1999**, *11*, 1281. Kimura, M.; Miki, N.; Adachi, N.; Tatewaki, Y.; Ohtaa, K.; Shiraiab, H. *J. Mater. Chem.* **2009**, *19*, 1086. Chen, J.; Liu, H.; Weimer, W. A.; Halls, M. D.; Waldeck, D. H.; Walker, G. C. *J. Am. Chem. Soc.* **2002**, *124*, 9034. Chen, J.; Ramasubramaniam, R.; Xue, C.; Liu, H. *Adv. Funct. Mater.* **2006**, *16*, 114. Zou, J.; Khondaker, S. I.; Huo, Q.; Zhai, L. *Adv. Funct. Mater.* **2009**, *19*, 479. Satishkumar, B. C.; Brown, L. O.; Gao, Y.; Wang, C.-C.; Wang, H.-L.; Doorn, S. K. *Nat. Nanotechnol.* **2007**, *2*, 560. Casagrande, T.; Imin, P.; Cheng, F.; Botton, G. A.; Zhitomirsky, I.; Adronov, A. *Chem. Mater.* **2010**, *22*, 2741. Baykal, B.; Ibrahimova, V.; Er, G.; Bengu, E.; Tuncel, D. *Chem. Commun.* **2010**, *46*, 6762. Deria, P.; Sinks, L. E.; Park, T. H.; Tomezsko, D. M.; Brukman, M. J.; Bonnell, D. A.; Therien, M. J. *Nano Lett.* **2010**, *10*, 4192. Nish, A.; Hwang, J.-Y.; Doig, J.; Nicholas, R. J *Nat. Nanotechnol.* **2007**, *2*, 640.
(16) Cheung, W.; Chiu, P. L.; Parajuli, R. R.; Ma, Y. F.; Ali, S. R.; He, H. X. *J. Mater. Chem.* **2009**, *19*, 6465. Jung, S.; Cha, M.; Park, J.; Jeong, N.; Kim, G.; Park, C.; Ihm, J.; Lee, J. *J. Am. Chem. Soc.* **2010**, *132*, 10964. Chen, Y.; Yu, L.; Feng, X.-Z.; Hou, S.; Liu, Y. *Chem. Commun.* **2009**, 4106.

(17) Zhang, Z.; Che, Y.; Smaldone, R. A.; Xu, M.; Bunes, B. R.; Moore, J. S.; Zang, L. *J. Am. Chem. Soc.* **2010**, *132*, 14113.
(18) Dìlaz Costanzo, G.; Ledesma, S.; Mondragon, I.; Goyanes, S. *J. Phys. Chem. C* **2010**, *114*, 14347.
(19) Saini, V.; Li, Z.; Bourdo, S.; Dervishi, E.; Xu, Y.; Ma, X.; Kunets, V. P.; Salamo, G. J.; Viswanathan, T.; Biris, A. R.; Saini, D.; Biris, A. S. *J. Phys. Chem. C* **2009**, *113*, 8023. Lee, J. M.; Park, J. S.; Lee, S. H.; Kim, H.; Yoo, S.; Kim, S. O. *Adv. Mater.* **2011**, *23*, 629. Qiu, L.; Yang, X.; Gou, X.; Yang, W.; Ma, Z.-F.; Wallace, G. G.; Li, D. *Chem.—Eur. J.* **2010**, *16*, 10653. Park, Y. D.; Lim, J. A.; Yunseok, J. A.; Hwang, M.; Lee, H. S.; Lee, D. H.; Lee, H. J.; Baek, J. B.; Cho, K. *Org. Electron.* **2008**, *9*, 317. Ehli, C. O. C.; Guldi, D.; Mateo-Alonso, A.; Prato, M.; Schmidt, C.; Backes, C.; Hauke, F.; Hirsch, A. *Natur. Chem.* **2009**, *1*, 243.
(20) Nobusawa, K.; Ikeda, A.; Kikuchi, J.; Kawano, S.; Fujita, N.; Shinkai, S. *Angew. Chem., Int. Ed.* **2008**, *47*, 4577.
(21) O'Connell, M. J.; Boul, P.; Ericson, L. M.; Huffman, C.; Wang, Y.; Haroz, E.; Kuper, C.; Tour, J.; Ausman, K. D.; Smalley, R. E. *Chem. Phys. Lett.* **2001**, *342*, 265.
(22) Ling, I.; Alias, Y.; Makha, M.; Raston, C. L. *New J. Chem.* **2009**, *33*, 1583.
(23) Chen, R. J.; Zhang, Y. G. *J. Phys. Chem. B* **2006**, *110*, 54. Chen, G.; Wright, P. M.; Geng, J.; Mantovani, G.; Haddleton, D. M. *Chem. Commun.* **2008**, 1097. Ikeda, A.; Totsuka, Y.; Nobusawa, K.; Kikuchi, J. *J. Mater. Chem.* **2009**, *19*, 5785. Quintana, M.; Prato, M. *Chem. Commun.* **2009**, 6005.
(24) Brunsveld, L.; Folmer, B. J. B.; Meijer, E. W.; Sijbesma, R. P. *Chem. Rev.* **2001**, *101*, 4071. Greef, T. F. A.; Meijer, E. W. *Nature* **2008**, *453*, 171.
(25) Gonzalez-Rodriguez, D.; Schenning, A. P. H. J. *Chem. Mater.* **2011**, *23*, 310. Palmer, L. C.; Stupp, S. I. *Acc. Chem. Res.* **2008**, *41*, 1674.
(26) Sijbesma, R. P.; Meijer, E. W. *Chem. Commun.* **2002**, 5. Hunter, C. A.; Ihekwaba, N.; Misuraca, M. C.; Segarra-Maset, M. D.; Turega, S. M. *Chem. Commun.* **2009**, 3964. Hunter, C. *Nature* **2011**, *469*, 39. Wilson, A. J. *Soft Matter* **2007**, *3*, 409. Lehn, J. M. *Polym. Int.* **2002**, *51*, 825.
(27) Yoosaf, K.; Belbakra, A.; Llanes-Pallas, A.; Bonifazi, D.; Armaroli, N. *Pure Appl. Chem.* **2011**, *83*, 899.
(28) Mohnani, S.; Llanes-Pallas, A.; Bonifazi, D. *Pure Appl. Chem.* **2010**, *82*, 917.
(29) Hoeben, F. J. M.; Herz, L. M.; Daniel, C.; Jonkheijm, P.; Schenning, A. P. H. J.; Silva, C.; Meskers, S. C. J.; Beljonne, D.; Phillips, R. T.; Friend, R. H.; Meijer, E. W. *Angew. Chem., Int. Ed.* **2004**, *43*, 1976. Friese, V. A.; Kurth, D. G. *Coord. Chem. Rev.* **2008**, *252*, 199. Antonietti, M. *Nat. Mater.* **2003**, *2*, 9.
(30) Chichak, K. S.; Star, A.; Altoé, V. P.; Stoddart, J. F. *Small* **2005**, *1*, 452.
(31) Ikea, A.; Tanaka, Y.; Nobusawa, K.; Kikuchi, J. *Langmuir* **2007**, *23*, 1091.
(32) Yoosaf, K.; Llanes-Pallas, A.; Marangoni, T.; Belbakra, A.; Marega, R.; Botek, E.; Champagne, B.; Bonifazi, D.; Armaroli, N. *Chem.—Eur. J.* **2011**, *17*, 3262.
(33) Llanes-Pallas, A.; Palma, C. A.; Piot, L.; Belbakra, A.; Listorti, A.; Prato, M.; Samorì, P.; Armaroli, N.; Bonifazi, D. *J. Am. Chem. Soc.* **2009**, *131*, 509.
(34) Llanes-Pallas, A.; Matena, M.; Jung, T.; Prato, M.; Stohr, M.; Bonifazi, D. *Angew. Chem., Int. Ed.* **2008**, *47*, 7726.
(35) Cabot, R.; Hunter, C. A.; Varley, L. M. *Org. Biomol. Chem.* **2010**, *8*, 1455. Cook, J. L.; Hunter, C. A.; Low, C. M. R.; Perez-Velasco, A.; Vinter, J. G. *Angew. Chem., Int. Ed.* **2007**, *46*, 3706. Cook, J. L.; Hunter, C. A.; Low, C. M. R.; Perez-Velasco, A.; Vinter, J. G. *Angew. Chem., Int. Ed.* **2008**, *47*, 6275.
(36) Yoosaf, K.; Belbakra, A.; Armaroli, N.; Llanes-Pallas, A.; Bonifazi, D. *Chem. Commun.* **2009**, 2830.
(37) Marangoni, T.; Mezzasalma, S. A.; Llanes-Pallas, A.; Yoosaf, K.; Armaroli, N.; Bonifazi, D. *Langmuir* **2011**, *27*, 1513.